Discretized disorder in planar semiconductor microcavities: Mosaicity effect on resonant Rayleigh scattering and optical parametric oscillation

Marco Abbarchi,[1,*] Carole Diederichs,[1] Ludovic Largeau,[2] Vincenzo Ardizzone,[1] Olivia Mauguin,[2] Timothee Lecomte,[1] Aristide Lemaitre,[2] Jacqueline Bloch,[2] Philippe Roussignol,[1] and Jerome Tignon[1]

[1]*Laboratoire Pierre Aigrain, École Normale Supérieure, Centre National de la Recherche Scientifique (UMR 8551), Université Pierre et Marie Curie, Université D. Diderot, FR-75231 Paris Cedex 05, France*

[2]*Laboratoire de Photonique et de Nanostructures, Centre National de la Recherche Scientifique, Route de Nozay, FR-91460 Marcoussis, France*

(Received 19 June 2011; revised manuscript received 22 November 2011; published 18 January 2012; corrected 25 January 2012)

The features of resonant secondary emission by two-dimensional multiple semiconductor microcavities are experimentally investigated. The multiband photonic/polaritonic dispersion makes possible a normal laser incidence which represents an isotropic probe of the system defectivity. We show that the static disorder determines the final states of the resonant Rayleigh scattering in the high-symmetry axes of the GaAs matrix. Scanning transmission electron microscopy and x-ray-diffraction measurements reveal the origins of disorder: a small misfit dislocation density and step formation at the layer interfaces due to strain accumulation and relaxation. These mosaicity effects ruled by the symmetry of the underlying GaAs matrix are common features of thick and strained crystals and determine the scattering channels by selecting the crystallographic discretized directions. The structural characterization demonstrates that, while the presence of misfit dislocations plays a minor role, the principal source of disorder is due to the elastic relaxation of strain. Moreover, interband optical parametric oscillation of the intensity balanced signal and idler beams is seeded by the resonant Rayleigh scattering and takes place in the directions selected by the photonic disorder in the distributed Bragg reflector.

DOI: 10.1103/PhysRevB.85.045316 PACS number(s): 78.66.−w, 71.36.+c, 78.35.+c, 72.10.Fk

I. INTRODUCTION

Static disorder in semiconductor heterostructures and its features in light-matter interaction[1] have been the subject of intense research in the past years, and it is now well known that the disorder has a strong impact in the physics of multilayered structures such as quantum wells (QWs)[2] or two-dimensional microcavities (2D-MCs).[3] The problem of interface roughness received particular attention, being a major issue ruling the relaxation of the in-plane translational invariance and thus allowing for changes in the wave vector of the exciton/polariton and limiting the coherence.[1–4]

Dielectric fluctuation induced by disorder strongly affects the coherent part of the secondary emission [the resonant Rayleigh scattering (RRS)],[1,4] which, in a first stage, attracted much attention, being a very fine probe of potential fluctuation in QWs.[1,2,4] Later studies put in evidence the features of RRS in QWs coupled to 2D-MCs, highlighting the relevant influence of disorder in the distributed Bragg reflectors.[5] It is a common opinion that dislocations in the distributed Bragg reflectors dominate the photonic disorder even if direct evidences are lacking.[3,5–8]

In high-quality 2D-MCs we can distinguish between two exciton/photon coupling regimes ruling the optical properties of the system:[3] (i) for small exciton-photon detuning the system may be described in terms of normal modes of coupled oscillators which are called polaritons, half-light and half-matter quasiparticles, and the regime is called strong coupling (SC), and (ii) for large exciton-photon detuning, where the SC features are washed out, the emission of the cavity can be described by photonic modes (CMs), and the system is in a weak coupling (WC) regime. In any case, due to the steep band dispersion of polaritonic or photonic bands, the RRS appears as an annular emission in the far field of the resonant secondary emission.[5,8,9]

In conventional experiments on semiconductor microcavities the excitation of intraband RRS was obtained only at specific azimuthal angles, conditioning the accessible final states and limiting the investigation of disorder related phenomena.[5,9] In this article we precisely address the origin of photonic disorder in the distributed Bragg reflectors by using a different approach based on multiple 2D-MC (2D-MMC), allowing for a better insight. Thanks to the multiplicity of the CMs, the resonant laser pump can be at normal incidence, thus potentially exciting the interband RRS in any accessible in-plane direction. It is the static disorder of the system that *chooses* a specific elastic scattering channel.

We investigate the far-field emission of two 2D-MMCs and its power dependence. At low incident power and large detuning (linear regime) the RRS ring presents strong anisotropies visible as twin speckles in well-defined directions, usually parallel to the main crystallographic in-plane directions [110] and [1-10]. High-angle annular dark field scanning transmission electron microscopy and x-ray diffraction demonstrate a mosaicity effect[10] in the structure layers, explaining the origin of the very peculiar speckle pattern in the RRS ring. The presence of misfit dislocations is found to play a minor role, while the microscopic tilt due to steps formation leading to a broadening of the x-ray-diffraction pattern is the main source of disorder.

The study of the secondary emission in the high-excitation regime and small detuning (nonlinear regime) shows the onset of optical parametric oscillation (OPO) seeded by the RRS in the same directions imposed by the underlying lattice geometry. Nevertheless, other directions for the OPO are possible when different kinds of defects are present.

The paper is organized as follows: in Sec. II we give a short description of the samples in analysis and of the experimental arrangement; in Sec. III we show the experimental results of spectroscopic and structural investigation by RRS, STEM, and x-ray-diffraction imaging; in Sec. IV we draw the conclusions.

II. SAMPLE GROWTH AND EXPERIMENTAL METHODS

Two 2D-MMCs samples, labeled as A and B, are grown in a molecular-beam epitaxy reactor. A cross section of sample A obtained by high-angle annular dark field scanning transmission electron microscopy (HAADF-STEM) (images are registered with an JEOL 2200 FS microscope) is shown in Fig. 1(a), while a magnified view of the central cavity is shown Fig. 1(b).[11] Three GaAs λ cavities (MC1, MC2, and MC3 from top to bottom) are embedded between GaAs/AlAs distributed Bragg reflectors and are separated by equal intermediate distributed Bragg reflectors. The number of GaAs/AlAs layers in the distributed Bragg reflectors from bottom to top is 15/11.5/11.5/18.5 for sample A and 13/13.5/13.5/13 for sample B, bringing us to a different Q factor (1350 for sample A and 740 for sample B). In sample A (sample B), nine (one) $In_{0.07}Ga_{0.93}As$ QWs (width 8.5 ± 0.3 nm) are placed at the antinodes of the electromagnetic field, determining the excitonic transition at ∼1.468 eV (∼1.457 eV) at 6 K. A scheme of the sample is shown in Fig. 1(c), together with the experimental implementation of spectroscopic characterization. A wedge in MC1 and MC3 thickness [the angles α and β in Fig. 1(c)] is introduced in order to control the relative energies of the individual CMs and of the detuning δ with respect to the excitonic transition [here we define the detuning δ as the energy difference between the excitonic transition and the energy minimum of the lowest cavity mode: $\delta = E_X - E_1(k = 0)$]. For relatively small δ, in the SC regime, the measured vacuum Rabi splitting is ∼10.4 meV for sample A and ∼3.6 meV for sample B. The dispersion in energy-momentum space of coupled photonic/polaritonic bands is represented in Fig. 1(d). The characterization of band dispersion in energy-momentum space of the 2D-MMC under nonresonant excitation (not shown)[11] demonstrates the presence of three photonic CMs [labeled as 1, 2, and 3 in Fig. 1(d)].

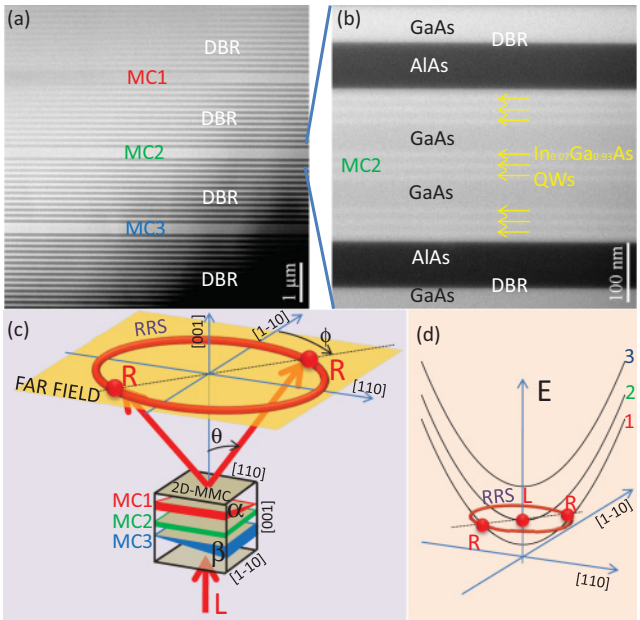

FIG. 1. (Color online) (a) HAADF-STEM image of sample A. (b) Magnified view of MC1 of sample A. The different layers are labeled, and the yellow arrows indicate the $In_{0.07}Ga_{0.93}As$ QWs. (c) Scheme of 2D-MMC (the distributed Bragg reflectors are not represented) and of the experimental configuration of excitation/detection of the far field. The angles α and β represent the cavity wedges. (d) Cavity modes/lower polariton state dispersions in energy-momentum space. The circle represents the possible final states of the RRS, while dots and arrows specify a particular scattering process $2(0,0) \rightarrow 1(+k,-k)$ labeled as R.

The CW excitation is provided by a tunable Ti:Sapphire laser focused normal to the sample surface [see Fig. 1(c)] on a spot of ∼40 μm [full width at half maximum (FWHM)]. The laser polarization is set linear. The sample is cooled down to 6 K in a cold-finger, liquid-Helium cryostat. The secondary emission collected in the far field is discriminated in polarization before detection.

By exciting interband energy degenerate scattering processes $2(0,0) \rightarrow 1(+k,-k)$ from the bottom of band 2 at $k_{\parallel} = 0$ we probe all the possible in-plane final states belonging to band 1 [see Figs. 1(c) and 1(d), where the possible final states for the RRS are represented by an isoenergetic ring, while specific scattering channels are represented by dots labeled as R on the ring]. Note that in the following we will deal only with MC1 and MC2 and we will neglect MC3, which does not play any role in this experiment.

Differently from state-of-the-art RRS experiments in 2D-MCs, the present system offers the big advantage of normal incidence excitation. Besides a simpler implementation of the experimental setup, this distinctive property of 2D-MMCs is essential for the study of RRS since it allows exciting along a high-symmetry axis of the system [parallel to the crystallographic growth direction [001] as shown in Fig. 1(c)]. Most importantly, this kind of experimental configuration represents an isotropic probe producing interband RRS and sampling the full extension of the elastic ring [see Figs. 1(c) and 1(d)]. Figure 1(c) describes the experimental arrangement: the collection of transmitted secondary emission is made in the far field by imaging the RRS ring on a silicon based CCD camera. Moreover, by selecting a single speckle R in the far field with an iris, we can measure the transmitted RRS intensity with a silicon based photodiode for a quantitative analysis. We choose a reference frame where the crystallographic directions [1-10] and [110] correspond to $\phi = 0$ and 90 deg, respectively [see Fig. 1(c)].

III. EXPERIMENTAL RESULTS AND DISCUSSION

A. Resonant Rayleigh scattering

Figures 2(a)–2(c) show the 2D-MMC far-field emission pattern for different detunings δ under resonant excitation of mode 2 at $k_{\parallel} = 0$ in the linear regime (excitation power ∼KW/cm^2). The strong emission at $\theta = 0$ deg is laser light transmitted through the sample. Figure 2(d) shows a typical power dependence of a single speckle.

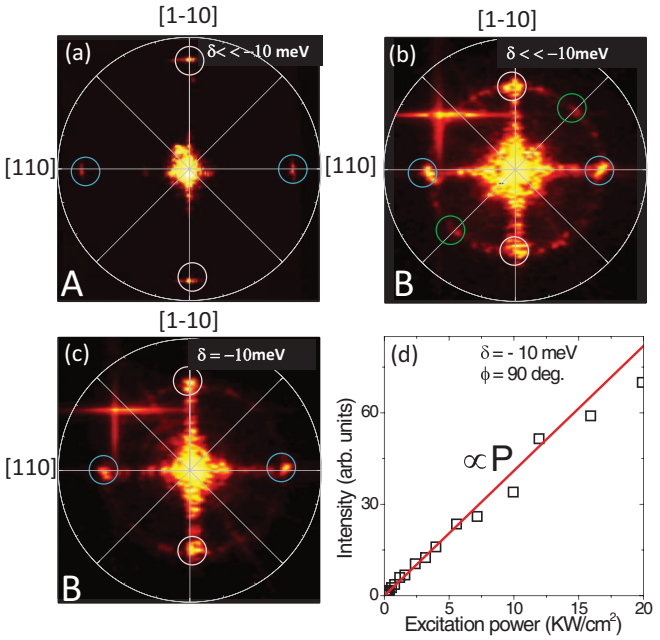

FIG. 2. (Color online) RRS ring from sample A (a) and sample B (b) and (c), as measured in the process $2(0,0) \rightarrow 1(+k,-k)$ for different δ and low incident power. The cross-shaped emission at $\phi \simeq 315$ deg in graphs (b) and (c) is stray light entering in the system. (d) Symbols: intensity of the speckle at $\phi = 90$ deg of graph (c) as a function of the incident power. The line is a linear fit to the data.

Distinctive features of the detected secondary emission in samples A and B are summarized as follows: (i) the secondary emission shows a polarization parallel to that of the incident laser, (ii) in all the investigated conditions the ringlike emission (the aperture is generally between $\theta \simeq 12$ and 15 deg in the investigated conditions) is anisotropic and structured in a speckle pattern, and (iii) the intensity of a single speckle increases linearly with respect to the incident laser power [see the linear fit to data in Fig. 2(d)]. Based on this evidence we interpret the resonant secondary emission as RRS induced by static disorder in the 2D-MMC. These results, which are obtained for large negative detuning ($\delta \ll 0$), where the modes are prevalently photonic, account for a relevant contribution to the disorder in the distributed Bragg reflectors.

The speckle pattern is centrally symmetric: for each speckle at a definite angle ϕ a twin speckle is present at $\phi + 180$ deg [as highlighted by circles of the same color around two twin speckles in Figs. 2(a)–2(c)]. Most important, the directions identified by two twin speckles, which recurrently appear in several measurements and in different experimental conditions, are not randomly distributed all along the RRS ring but tend to coalesce in specific in-plane directions: the brightest speckles appear in correspondence of the directions of the high-symmetry axes of the GaAs matrix [i.e., [110] and [1-10]]. At the margin we note that different directions of the RRS are possible, as shown in Fig. 2(b), where the speckles with lower intensities at $\phi = 45$ and 225 deg correspond to the crystallographic direction [100]. We conclude that disorder in the Bragg mirrors is discretized and is influenced by the symmetry of the underlying GaAs matrix.

B. Structural characterization

In order to precisely address and clarify the origin of the disorder responsible for the RRS we performed TEM and STEM at the layer interface and high-resolution x-ray-diffraction measurements with a triple axis PANalytical XPert Pro diffractometer. Figure 3(a) is a 220 dark field TEM image where a dislocation is visible at the first interface substrate/DBR, while Fig. 3(b) is a high-resolution view of the defect. This is the result of plastic relaxation inducing a misfit dislocation, which in turn results in a threading dislocation (not visible in the plane of view) propagating across the microcavity. The density of this dislocation ($\sim$1 dislocation every 3 μm) is much smaller than that expected for a completely relaxed structure ($\sim$1 dislocation every 250 nm), suggesting that the main mechanism of strain relaxation is not due to nucleation of dislocations.

Figures 3(c)–3(e) show HAADF-STEM images of the substrate/DBR interfaces (vertical and horizontal axes in

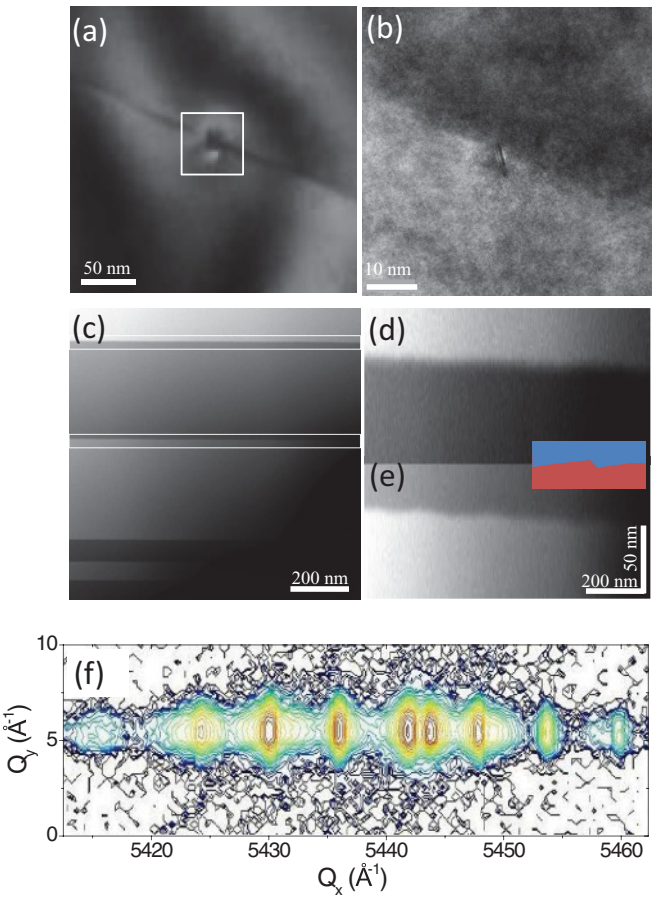

FIG. 3. (Color online) (a) 220 dark field TEM image of sample A at the first interface substrate/DBR. The white square indicates the area shown in graph (b). (b) High-resolution TEM image of the misfit dislocation shown in (a). (c) HAADF-STEM image of cavity A at the first interface substrate/DBR. The horizontal white lines indicate the areas shown in graphs (d) and (e). (d) and (e) Expanded view of the areas selected in graph (c). Vertical and horizontal axes have different scales in order to evidence the layer tilts. The inset shows a scheme of the layer arrangement. (f) High-resolution x-ray reciprocal space mapping of sample B around the 004 reflection.

Figs. 3(d) and 3(e) are intentionally rescaled in order to highlight the sharp features). The periodicity of the ondulation is hundreds of nanometers and, as we show below, this periodic mosaicity is also observed in x-ray-diffraction measurements. This effect is the resulting step formation and bunching due to elastic accommodation of the strain.

Typical diffraction reciprocal space mapping (RSM) around the 004 reflection obtained by high-resolution x-ray-diffraction measurements is shown in Fig. 3(f). The RSM is shown in the reciprocal lattice units ($Å^{-1}$). The horizontal Q_x axis is parallel to the [001] growth direction and the vertical Q_y axis is parallel to the [110] in-plane direction. The periodic peaks correspond to diffraction of the distributed Bragg reflectors' periodic superlattice epitaxial layers, while the nonperiodic peak corresponds to the 004 diffraction of the substrate. The peaks' broadening, due to slight deviations of the 004 reciprocal space vector, is associated to a tilt of the crystallographic planes forming misoriented domains.[10] The formation of steps at the interfaces induces the tilt of the crystallographic planes, resulting in misoriented blocks, domains comparable to a mosaic. From the peaks' full width at half maximum measured on four RSMs, we estimate a coherence length of hundreds of nanometers. The coherence length as deduced by the RSM packs' broadening is ∼500 and ∼800 nm along the preferential [110] and [1-10] in-plane directions for sample A, while it is ∼400 nm for both directions in sample B. X-ray RSM around inclined reflections (not shown here) show the same broadening of the diffracted peaks and indicate that the lattice parameters in the plane of the layers is the same over whole the structure. This also suggests that few misfit dislocations are present inside the structure and corroborates that only a small part of the strain has been accommodated by nucleation of dislocations.

This structural long-range disorder is typical of thick and strained crystals such as 2D-MCs. From the comparison with HAADF-STEM analysis we conclude that the main scattering mechanism is associated to microscopic tilts; in fact the distances deduced by the RSM are consistent with the ondulations shown in Figs. 3(d) and 3(e), much smaller than the distance between misfit dislocations. We conclude that the microscopic tilts associated to the step formation is the main source of disorder in the distributed Bragg reflectors and justify the peculiar far-field pattern observed in the RRS ring.

C. Optical parametric oscillation

Besides disorder related phenomena, a major subject of investigation in 2D-MCs is the generation of optical parametric oscillation.[11–16] It is now well established that strong χ^3-polaritonic/excitonic nonlinearity can give rise to parametric phenomena[11–16] and that intensity balanced signal and idler (S and I) beams can be produced in energy degenerate interband processes under normal incidence excitation.[17] For this reason we performed measurements of resonant secondary emission at small detuning under high incident power (nonlinear regime).

In the same experimental conditions previously described, we investigate the far field of twin speckles for $\delta \simeq 0$ meV in sample A. As previously shown for the linear excitation

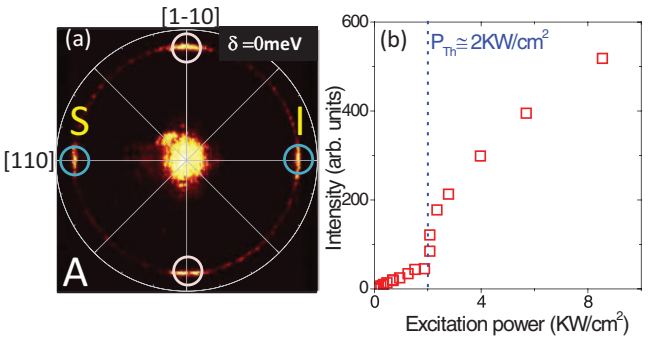

FIG. 4. (Color online) (a) Far-field pattern for the interband scattering $2(0,0) \rightarrow 1(+k,-k)$ under high excitation power for sample A. (b) Symbols: S intensity as a function of the incident power. The vertical dashed line labels the threshold power P_{Th}.

regime, the far-field pattern shows strong anisotropies [see Fig. 4(a)] being characterized by twin speckles in the directions [110] and [1-10]. The power dependence shows a thresholdlike trend: below a threshold power ($P_{Th} = 2$ KW/cm^2) the emission is dominated by incoherent secondary emission and RRS, while after the threshold the emission intensity abruptly changes its slope with a nonlinear trend. This is the signature of the onset of interband optical parametric oscillation, as already reported in previous works.[11,17] Here, the resonant excitation of interband parametric scattering of two incident photons at $k_{\parallel} = 0$ is ruled by the phase-matching conditions: S and I are degenerate in energy with respect to the pump, which is resonant with the bottom band 2(0,0), and have opposite in-plane momentums, coincident with the crystallographic directions.[17]

On the basis of this evidence we conclude that the same disorder in the distributed Bragg reflectors responsible for the RRS determines the possible final states of parametric scattering and optical parametric oscillation. This implies that a specific mode of the coherent oscillation of S and I is seeded by the RRS scattering and stabilized in a well-defined mode, avoiding undesired mode hopping and reducing the oscillation threshold to very small values differently from a perfectly isotropic system.

We stress that all these features can be easily evidenced thanks to the symmetric configuration of excitation, which does not condition the final states of the RRS or parametric scattering. We mention that the influence of directional static disorder in intraband optical parametric oscillation has already been reported in real-space imaging experiments, suggesting a strain relaxation due to the lattice mismatch of the AlAs layers in the distributed Bragg reflectors[16] in analogy with similar evidences in RRS experiments.[5,18] The dominant source of disorder was believed to be misfit dislocations in the thick and strained distributed Bragg reflectors.

For the sake of thoroughness we report a last case of directional disorder influencing the optical parametric oscillation eventually found when addressing specific points on sample B.

Despite the high optical quality of the investigated samples, real-space imaging of resonant transmission [see the inset of Fig. 5(a)] occasionally reveals the presence of long line-shaped defects. When focusing the excitation on this kind of

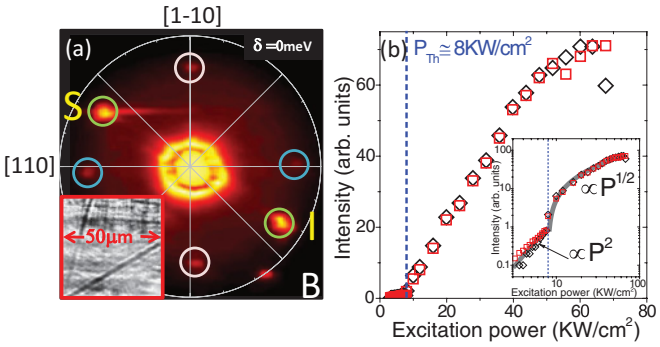

FIG. 5. (Color online) (a): Far-field pattern for the interband scattering $2(0,0) \rightarrow 1(+k,-k)$ under high excitation power for sample B. Inset: real-space image of resonant transmission. (b) Symbols: S and I intensity as a function of the incident power. The vertical dashed line labels the threshold power P_{Th}. Inset: same as (b) in logarithmic scales. Lines are quadratic (below P_{Th}) and square-root (over P_{Th}) fit to the data.

defects the corresponding far-field emission shows, besides the usual [110] and [1-10] directions determined by the mosaicity, much stronger emission in directions different from the crystallographic axes [see a representative example in Fig. 5(a), where S and I at ∼127–307 deg are shown]. Power dependence measurements on S and I [see Fig. 5(b)] show the onset of optical parametric oscillation suggesting that sources of disorder other than mosaicity dominate determining the final states of the scattering channels. Tentatively, we attribute this kind of disorder to surface defects or threading dislocations.

We note that the parametric nature of the two-photon process agrees well with theoretical predictions and experimental evidences:[12,13] at low excitation power the twin beam intensity increases quadratically with the incident power and at a threshold value abruptly changes its slope, following a square-root dependence [see the quadratic and square-root fit to the data in the inset of Fig. 5(b)]. Note that threshold power P_{Th} for OPO increases when going to negative detuning.[19] This is why we only observe RRS in Fig. 2 (at very large negative detuning, $\delta \ll 0$) and for similar excitation powers OPO in Figs. 4 and 5 (at zero detuning, $\delta = 0$).[12] Most important, S and I beams are intrinsically balanced in intensity, a very attractive feature for quantum optics applications of parametric scattering and optical parametric oscillation in semiconductor nanostructures.[17,20]

IV. CONCLUSION

In this paper we have shown that a mosaicity effect in the distributed Bragg reflectors rules the disorder in 2D-MCs and strongly affects the far-field features of the secondary emission, the main source of disorder being an elastic accommodation of the strain. The accumulation and relaxation of strain along the high-symmetry axes of the crystal determine the RRS along the same directions in different conditions of exciton-photon detuning and/or coupling. In the nonlinear excitation regime, intensity balanced optical parametric oscillation of S and I beams takes place along the same crystallographic directions being seeded in specific modes by the directional RRS. Nevertheless, other directions are accessible to the OPO when the defectivity determines a strong anisotropy in a defined scattering channel.

In conclusion, we remark that the recent quality improvement in the fabrication techniques of epitaxial materials enabled the demonstration of surprising quantum effects in polariton physics. Striking phenomena such as polariton condensation[21] and superfluidity,[8] quantized vortices[22] and soliton formation,[23] Josephson oscillations,[24] as well as parametric scattering phenomena[11–17] have been recently shown. If on one side the high optical quality of the microcavities relies on the reduced defectivity that is detrimental for the radiative emission properties, on the other side the presence of residual disorder is at the base of the observation of the mentioned effects. In this sense the study of the ultimate sources of disorder in microcavities can help the understanding and the exploitation of these peculiar phenomena.

ACKNOWLEDGMENTS

We thank Alberto Amo for fruitful discussions. This work was partly supported by the ANR contract "GEMINI" (Grant No. ANR-07-NANO-005) and by the FP7 ITN "Clermont4" (235114).

*marco.abbarchi@lpa.ens.fr

[1] J. Hegarty, M. D. Sturge, C. Weisbuch, A. C. Gossard, and W. Wiegmann, Phys. Rev. Lett. **49**, 930 (1982); M. Gurioli, F. Bogani, S. Ceccherini, and M. Colocci, *ibid.* **78**, 3205 (1997); X. Marie, P. Le Jeune, T. Amand, M. Brousseau, J. Barrau, M. Paillard, and R. Planel, *ibid.* **79**, 3222 (1997); S. Haacke, R. A. Taylor, R. Zimmermann, I. Bar-Joseph, and B. Deveaud, *ibid.* **78**, 2228 (1997); M. Woerner and J. Shah, *ibid.* **81**, 4208 (1998); D. Birkedal and J. Shah, *ibid.* **81**, 2372 (1998).

[2] E. Runge, *Solid State Physics, Excitons in Semiconductors Nanostructures* (Academic, New York, 2002), Vol. 57; C. Klingshirn, *Semiconductor Optics*, 2nd ed. (Springer-Verlag, New York, 2005).

[3] J. Baumberg and L. Vina, Semicond. Sci. Technol. **18**, S279 (2003); A. V. Kavokin, J. J. Baumberg, G. Malpuech, and F. P. Laussy, *Microcavities* (Oxford University Press, New York, 2007).

[4] W. Langbein, J. M. Hvam, and R. Zimmermann, Phys. Rev. Lett. **82**, 1040 (1999); P. Bozsoki, P. Thomas, M. Kira, W. Hoyer, T. Meier, S. W. Koch, K. Maschke, I. Varga, and H. Stolz, *ibid.* **97**, 227402 (2006).

[5] M. Gurioli, F. Bogani, D. S. Wiersma, Ph. Roussignol, G. Cassabois, G. Khitrova, and H. Gibbs, Phys. Rev. B **64**, 165309 (2001); W. Langbein and J. M. Hvam, Phys. Rev. Lett. **88**, 047401 (2002); W. Langbein, J. Phys. Condens. Matter **16**, S3645 (2004); M. Gurioli, F. Bogani, L. Cavigli, H. Gibbs, G. Khitrova, and D. S.

Wiersma, Phys. Rev. Lett. **94**, 183901 (2005); W. Langbein, Riv. Nuovo Cimento **33**, 255 (2010).

[6]A. V. Shchegrov, J. Bloch, D. Birkedal, and J. Shah, Phys. Rev. Lett. **84**, 3478 (2000); F. M. Marchetti, J. Keeling, M. H. Szymanska, and P. B. Littlewood, *ibid.* **96**, 066405 (2006).

[7]M. M. Glazov and L. E. Golub, Phys. Rev. B **77**, 165341 (2008); T. C. H. Liew, C. Leyder, A. V. Kavokin, A. Amo, J. Lefrere, E. Giacobino, and A. Bramati, *ibid.* **79**, 125314 (2009); M. M. Glazov and L. E. Golub, *ibid.* **82**, 085315 (2010).

[8]I. Carusotto and C. Ciuti, Phys. Rev. Lett. **93**, 166401 (2004); A. Amo, D. Sanvitto, F. P. Laussy, D. Ballarini, E. del Valle, M. D. Martin1, A. Lemaitre, J. Bloch, D. N. Krizhanovskii, M. S. Skolnick, C. Tejedor, and L. Viña, Nature (London) **457**, 291 (2009).

[9]T. Freixanet, B. Sermage, J. Bloch, J. Y. Marzin, and R. Planel, Phys. Rev. B **60**, R8509 (1999); D. M. Whittaker, *ibid.* **61**, R2433 (2000); P. G. Savvidis, J. J. Baumberg, D. Porras, D. M. Whittaker, M. S. Skolnick, and J. S. Roberts, *ibid.* **65**, 073309, (2002); M. Richard, J. Kasprzak, R. Romestain, R. André, and L. S. Dang, Phys. Rev. Lett. **94**, 187401 (2005).

[10]V. Holy, J. Kubena, E. Abramof, K. Lischka, A. Pesek, and E. Koppensteiner, J. Appl. Phys. **74**, 1736 (1993).

[11]C. Diederichs and J. Tignon, Appl. Phys. Lett. **87**, 251107, (2005); C. Diederichs, J. Tignon, G. Dasbach, C. Ciuti, A. Lematre, J. Bloch, Ph. Roussignol, and C. Delalande, Nature (London) **440**, 904 (2006).

[12]C. Ciuti, P. Schwendimann, B. Deveaud, and A. Quattropani, Phys. Rev. B **62**, R4825 (2000); C. Ciuti, P. Schwendimann, and A. Quattropani, *ibid.* **63**, 041303(R) (2001); D. M. Whittaker, *ibid.* **63**, 193305 (2001); C. Ciuti, P. Schwendimann, and A. Quattropani, Semicon. Sci. Tech. **18**, S279 (2003); J. Ph. Karr, A. Baas, and E. Giacobino, Phys. Rev. A **69**, 063807 (2004); A. Baas, J. P. Karr, H. Eleuch, and E. Giacobino, *ibid.* **69**, 023809 (2004); D. Taj, T. Lecomte, C. Diederichs, Ph. Roussignol, C. Delalande, and J. Tignon, Phys. Rev. B **80**, 081308 (2009).

[13]R. Butte, M. S. Skolnick, D. M. Whittaker, D. Bajoni, and J. S. Roberts, Phys. Rev. B **68**, 115325 (2003)

[14]Y. R. Shen, *The Principles of Nonlinear Optics* (Wiley, Hoboken, 2003).

[15]J. J. Baumberg, P. G. Savvidis, R. M. Stevenson, A. I. Tartakovskii, M. S. Skolnick, D. M. Whittaker, and J. S. Roberts, Phys. Rev. B **62**, R16247 (2000); R. Houdré, C. Weisbuch, R. P. Stanley, U. Oesterle, and M. Ilegems, Phys. Rev. Lett. **85**, 2793 (2000); M. Saba, C. Ciuti, J. Bloch, V. Thierry-Mieg, R. André, Le Si Dang, S. Kundermann, A. Mura, G. Bongiovanni, J. L. Staehli, and B. Deveaud, Nature (London) **414**, 731 (2003); W. Langbein, Phys. Rev. B **70**, 205301 (2004); D. N. Krizhanovskii, D. Sanvitto, A. P. D. Love, M. S. Skolnick, D. M. Whittaker, and J. S. Roberts, Phys. Rev. Lett. **97**, 097402 (2006); M. Romanelli, C. Leyder, J. Ph. Karr, E. Giacobino, and A. Bramati, *ibid.* **98**, 106401 (2007).

[16]D. Sanvitto, D. N. Krizhanovskii, D. M. Whittaker, S. Ceccarelli, M. S. Skolnick, and J. S. Roberts, Phys. Rev. B **73**, 241308(R) (2006).

[17]M. Abbarchi, V. Ardizzone, T. Lecomte, A. Lemaitre, I. Sagnes, P. Senellart, J. Bloch, Ph. Roussignol, and J. Tignon, Phys. Rev. B **83**, 201310(R) (2011).

[18]M. Gurioli, F. Bogani, D. S. Wiersma, Ph. Roussignol, G. Cassabois, G. Khitrova, and H. Gibbs, Phys. Status Solidi A **190**, 363 (2002).

[19]A detailed discussion of this topic is beyond the aim of the present investigation. A paper on this subject is in preparation.

[20]K. Edamatsu, G. Oohata, R. Shimizu, and T. Itoh, Nature **431**, 167 (2004); A. Baas, J.-Ph. Karr, M. Romanelli, A. Bramati, and E. Giacobino, Phys. Rev. Lett. **96**, 176401 (2006); S. Portolan, O. Di Stefano, S. Savasta, F. Rossi, and R. Girlanda, Phys. Rev. B **77**, 035433 (2008); **77**, 195305 (2008); J. U. Fürst, D. V. Strekalov, D. Elser, A. Aiello, U. L. Andersen, Ch. Marquardt, and G. Leuchs, Phys. Rev. Lett. **106**, 113901 (2011).

[21]J. Kasprzak, M. Richard, S. Kundermann, A. Baas, P. Jeambrun, J. M. J. Keeling, F. M. Marchetti, M. H. Szymańska, R. André, J. L. Staehli, V. Savona, P. B. Littlewood, B. Deveaud, and Le Si Dang, Nature (London) **443**, 409 (2006); D. Sanvitto, A. Amo, L. Viña, R. André, D. Solnyshkov, and G. Malpuech, Phys. Rev. B **80**, 045301 (2009).

[22]K. G. Lagoudakis, M. Wouters, M. Richard, A. Baas, I. Carusotto, R. André, D. L. S. Dang, and B. Deveaud-Peledran, Nat. Phys. **4**, 706 (2008); K. G. Lagoudakis, T. Ostatnicky, A. V. Kavokin, Y. G. Rubo, R. André, and B. Deveaud-Pledran, Science **326**, 974 (2009).

[23]A. Amo *et al.*, Science **332**, 1167 (2011); H. Flayac, D. D. Solnyshkov, and G. Malpuech, Phys. Rev. B **83**, 193305 (2011).

[24]K. G. Lagoudakis, B. Pietka, M. Wouters, R. André, and B. Deveaud-Pledran, Phys. Rev. Lett. **105**, 120403 (2010).